Journal of Controlled Release 235 (2016) 337–351

Contents lists available at ScienceDirect

Journal of Controlled Release

journal homepage: www.elsevier.com/locate/jconrel

Review article

DLS and zeta potential – What they are and what they are not?

Sourav Bhattacharjee

School of Veterinary Medicine, University College Dublin (UCD), Belfield, Dublin 4, Ireland

ARTICLE INFO

Article history:
Received 13 April 2016
Received in revised form 8 June 2016
Accepted 9 June 2016
Available online 10 June 2016

Keywords:
DLS
Zeta potential
Hydrodynamic radius
Surface potential
Colloid stability
Surface charge

ABSTRACT

Adequate characterization of NPs (nanoparticles) is of paramount importance to develop well defined nanoformulations of therapeutic relevance. Determination of particle size and surface charge of NPs are indispensable for proper characterization of NPs. DLS (dynamic light scattering) and ZP (zeta potential) measurements have gained popularity as simple, easy and reproducible tools to ascertain particle size and surface charge. Unfortunately, on practical grounds plenty of challenges exist regarding these two techniques including inadequate understanding of the operating principles and dealing with critical issues like sample preparation and interpretation of the data. As both DLS and ZP have emerged from the realms of physical colloid chemistry – it is difficult for researchers engaged in nanomedicine research to master these two techniques. Additionally, there is little literature available in drug delivery research which offers a simple, concise account on these techniques. This review tries to address this issue while providing the fundamental principles of these techniques, summarizing the core mathematical principles and offering practical guidelines on tackling commonly encountered problems while running DLS and ZP measurements. Finally, the review tries to analyze the relevance of these two techniques from translatory perspective.

Contents

Abbreviations: μ_e, electrophoretic mobility; A2M, alpha-2 macroglobulin; ACF, autocorrelation function; APD, Avalanche photo diode; apoA1, Apolipoprotein *A*1; BSA, bovine serum albumin; CCD, charge-coupled device; cP, centipoise; CTAB, cetyltriethylammoniumbromide; DCS, differential centrifugal sedimentation; DDS, drug delivery systems; DI, deionized; DLS, dynamic light scattering; DMEM, Dulbecco's modified Eagle's medium; DMSO, dimethyl sulfoxide; D_r, rotational diffusion coefficient; D_t, translational diffusion coefficient; EDL, electric double layer; EM, electron microscopy; EU, European Union; FCS, fetal calf serum; FTIR, Fourier-transform infrared spectroscopy; GNPs, gold nanoparticles; HB, hemoglobin; He, helium; HS, Helmholtz-Smoluchowski; HSA, human serum albumin; Ig, immunoglobulin; ITC, isothermal titration calorimetry; k_B, Boltzmann constant; kcps, kilo counts per second; KNO_3, potassium nitrate; mV, millivolts; mW, milliwatt; NaCl, sodium chloride; Ne, neon; NIBS, non-invasive backscatter system; NIST, National Institute of Standards and Technology (USA); NP, nanoparticle; NTA®, nanoparticle tracking analysis; PALS, phase analysis light scattering; PDI, polydispersity index; PEC, polyelectrolyte complex; PEG, polyethylene glycol; PLA, poly-lactic acid; PMMA, poly-methyl-methacrylate; RCF, raw correlation function; R_g, radius of gyration; R_H, hydrodynamic radius; RI, refractive index; RPMI, Roswell Park Memorial Institute medium; S/N, signal-to-noise; SAXS, small angle X-ray scattering; SLS, static light scattering; SMPS, scanning mobility particle sizer; SOP, standard operating protocol; T, absolute temperature; TEM, transmission electron microscopy; UHV, ultrahigh vacuum; ZP, zeta potential; ε_r, relative permittivity/dielectric constant; η, absolute viscosity.

E-mail address: sourav.bhattacharjee@ucd.ie.

http://dx.doi.org/10.1016/j.jconrel.2016.06.017
0168-3659/

1. Introduction

Physicochemical properties of nanomaterials contribute towards their behavior within biological milieu [1,2]. Hence, adequate characterization of the nanoparticles (NPs) is essential in order to obtain reliable data with high translatory output. This also becomes relevant due to the safety concerns which are often attributed to the physical (e.g., particle size [3], surface charge [4], shape [5]) and chemical (e.g., surface functionalization with different ligands including PEGylation [6], impurity [7], crystallinity [8]) properties of NPs. Sufficient characterization helps to explain the NPs as chemical species which are highly reactive and exhibit unprecedented characteristics compared to bulk materials (e.g., conductivity [9], fluorescence [10], magnetism [11]). To broaden the scope for applications of NPs, a research-intensive framework within the academia and industry has emerged and attracted significant funding plus media attention in last few years [12]. Surface charge and particle size are the two most commonly mentioned factors that are responsible for a range of biological effects of NPs including cellular uptake [13], toxicity [14] and dissolution [15]. Emerging data indicate the influence of these two factors in release profile from NPs designed to carry drug payloads (e.g., macromolecules [16], peptides [17]) and release at target sites (e.g., small intestine [18] for oral drug delivery purposes). It is important to investigate these two parameters during development of nanoparticulate DDS (drug delivery systems) especially given the fact that biological matrices are known to alter these two features of NPs with different mechanisms (e.g., protein adsorption causing the characteristic *corona* [19,20]).

DLS (dynamic light scattering) – also known as *photon correlation spectroscopy* [21] or *quasi-elastic light scattering* [22] - and ZP (zeta potential) have emerged as simple table-top techniques executable under ordinary lab environments to investigate the (hydrodynamic) size and surface charge of NPs, respectively. From techniques that were exclusively available to colloid chemists, both DLS and ZP have evolved into popular tools within pharmacy community. The integrated, compact and affordable instruments offer user-friendly digital interfaces along with possibility for comprehensive data analysis. Additionally, the techniques are non-invasive, require minimal sample preparation and no pre-experimental calibration. The modern instruments are able to guide the users on the quality of the generated data with possibility for time-dependent measurements and ability to export the data traces as files compatible with various plotting softwares.

Unfortunately, due to frequent use with lack of caution and proper training, the quality of the reported data with DLS and ZP in nanomedicine research is not always excellent. Dispersions of NPs in colloidal systems show dual phases (dispersed and dispersant), do not settle over time [23] and are characterized by *Brownian motion* of the particles [24]. For charged NPs the system becomes even more complex due to the interactions between surfaces, molecules and ions leading to the creation of adsorbed layers on NPs [25]. Both DLS and ZP utilize these properties of colloid dispersions in order to deduce the hydrodynamic radius (R_H) [26] and potential difference at the characteristic *slipping plane* of electrophoretically mobile particles [27]. In this review, an effort is made to offer a simple account on these two techniques while referring only to essential mathematical principles in order to understand their strengths and weaknesses. Succinct discussions are offered on why and how different factors influence these measurements which cumulatively determine the quality of the data. The review also tries to deliver realistic examples while touching practicalities of these techniques which are relevant for drug delivery.

2. DLS (dynamic light scattering)

2.1. Background

2.1.1. Particle size in defining nanomaterials

Size is an important factor to define NPs although considerable debate exists on the size threshold to distinguish NPs from bulk materials.

In order to address this issue, the EU (European Union) released a directive (2011/696/EU) which offered specific guidelines on how to define a *nanomaterial*. Some relevant excerpts from the document are:

(1) [Paragraph 8] "*A defined size range would facilitate a uniform interpretation. The lower limit was proposed at 1 nm. An upper limit of 100 nm is commonly used by general consensus, but there is no scientific evidence to support the appropriateness of this value. The use of a single upper limit might be too limiting for the classification of nanomaterials and a differentiate approach might be more appropriate.*"

(2) [Paragraph 9] "*The International Organisation for Standardisation defines the term 'nanomaterial' as 'material' with any external dimensions in the nanoscale or having internal structure or surface structure in the 'nanoscale'. The term 'nanoscale' is defined as size range of approximately 1 nm and 100 nm.*"

(3) [Paragraph 11] "*A nanomaterial as defined in this recommendation should consist for 50 % or more of particles having a size between 1 nm-100 nm.*"

Apart from providing legally binding definition of nanomaterials the document also gave clear guidelines on how to characterize them:

(4) [Paragraph 8] "*For regulatory purposes, the number size distribution should also be considered using the mean size and the standard deviation of the size to refine the definition. The size distribution of a material should be presented as size distribution based on the number concentration (i.e. the number of objects within a given size range divided by the number of objects in total) and not on the mass fraction of nanoscale particles in the nanomaterial as a small mass fraction may contain the largest number of particles.*"

There are few interesting propositions made in the document and it would be appropriate to understand DLS as a nanoparticulate size measuring tool from that perspective. The document relaxed the widely popular size threshold of 1–100 nm to be considered as nanomaterials although still defined *nanoscale* materials to have at least one external dimension ≤100 nm. Even a mixture of particles with different sizes can be considered as nanomaterials as long as <50% of the particles (by number) present are ≤100 nm. As a result it now becomes important to know the size distribution of the different population of particles within a mixture. Thirdly, not only there is a requirement to know precise size distribution but it is now equally important to know the number distribution of NPs in samples. These findings will become important while discussing DLS in subsequent sections.

2.1.2. Principles of DLS

2.1.2.1. Scattering of light by particles. Dispersed NPs scatter incident light proportional to the 6th power of their radii [28]. When the particles are <1/10th of the wavelength of the incident light (i.e. λ/10) in size, the scattered light carries same energy (elastic scattering) to the incident light and is not angle-dependent (*Rayleigh scattering*) [29]. However, when the size of the particles exceeds this threshold of λ/10 then Rayleigh scattering is replaced by anisotropic *Mie scattering* where the scattered light is unequal in energy (inelastic scattering) to the incident light and angle-dependent (Fig. 1) [30] where the scattered light is most intense towards the direction of the incident light [31]. This size threshold (λ/10) is due to the way electromagnetic waves (e.g., light) interact with a particle and falls beyond the scope of this review although excellent textbooks and reference literature are available for consultation [32,33].

2.1.2.2. Fundamental mathematical operators. Particles in a colloid dispersion scatter an incident laser and the intensity of the scattered light is detected in DLS. The continuously mobile particles within dispersion cause constructive and destructive interferences and hence, the intensity of scattered light fluctuates over time (Fig. 2A) [34]. In DLS the fluctuation of intensity in scattered light is correlated against short decay intervals (τ) and the intensity ACF (autocorrelation function) is obtained [35] through the following mono-exponential equation (Fig. 2B) for samples with purely monodisperse particles (Eq. (1)):

$$G(\tau) = 1 + b.e^{-2D_t q^2 \tau} \quad (1)$$

Here, b = constant dependent upon the instrument and settings of optics, D_t = translational diffusion coefficient and q = scattering vector which can further be expressed as (Eq. (2)):

$$|q| = \frac{4\pi n_o}{\lambda_o \, sin\frac{\theta}{2}} \quad (2)$$

where, n_o = refractive index (RI) of the solvent, λ_o = wavelength in vacuum and θ = scattering angle.

The intensity ACF (G(π)) is often written as G2(τ) and is expressed as a function of field correlation function G1(τ) as mentioned in the following Eq. (3):

$$G2(\tau) = 1 + G1(\tau)^2 \quad (3)$$

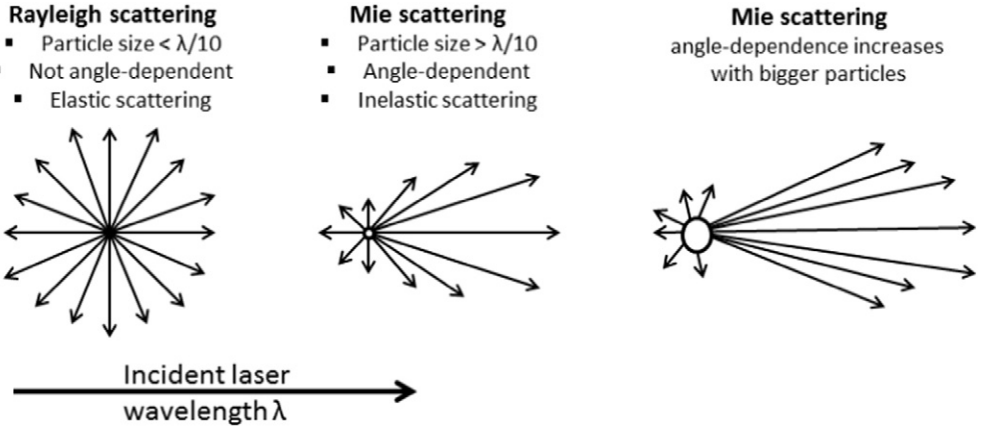

Fig. 1. Schematic showing the differences between Rayleigh and Mie scattering.

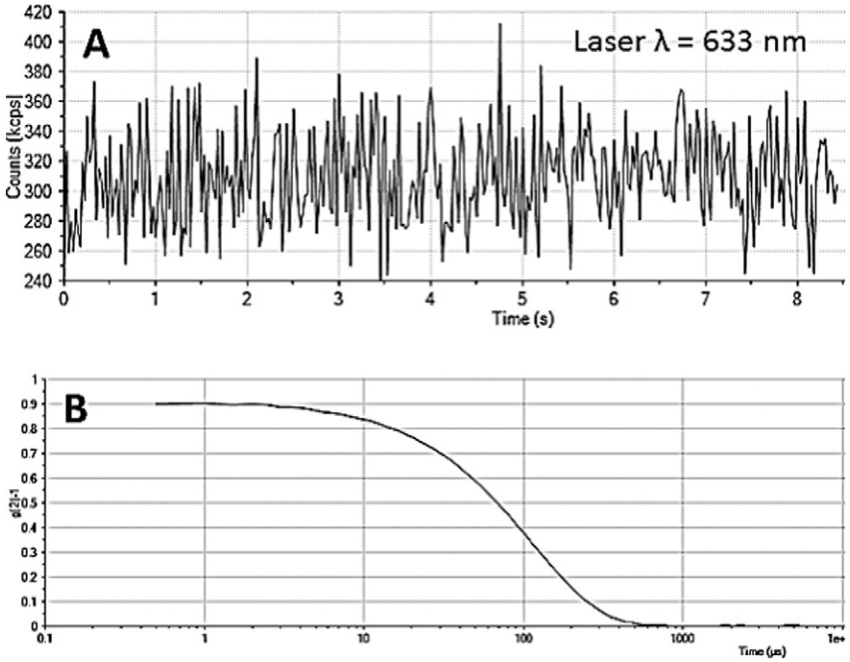

Fig. 2. (A) Fluctuation in intensity of the scattered light by NPs during DLS due to constructive and destructive interferences. (B) The correlogram generated by the software in order to estimate the R_H. The results are from DLS measurements performed at 25 °C on highly monodisperse 100 nm carboxylated latex beads (PDI 0.01) dispersed in water (100 μg/ml) in Malvern NanoZS instrument using plastic cuvettes (DTS1070) and analyzed by Zetasizer® (version 7.10) software.

In DLS instruments (e.g., Malvern Zetasizer®) a correlogram is generated where RCF (raw correlation function) is plotted (Fig. 2B) against delay time (τ) as shown in Eq. (4):

$$RCF = G2(\tau) - 1 = G1(\tau)^2 \tag{4}$$

which shows that the RCF is dependent on the field correlation function G1(τ).

The autocorrelation functions [G2(τ) or G2(τ) – 1] in DLS are calculated by data fitting and then the D_t is calculated using Eq. (1). The hydrodynamic radius (R_H) of solid spherical particles can be derived as shown in Eq. (5) (*Stokes-Einstein equation*):

$$D_t = \frac{k_B T}{6\pi\eta R_H} \tag{5}$$

Where k_B = Boltzmann constant ($1.38064852 \times 10^{-23}$ J/K), T = temperature, η = absolute viscosity and R_H = hydrodynamic radius.

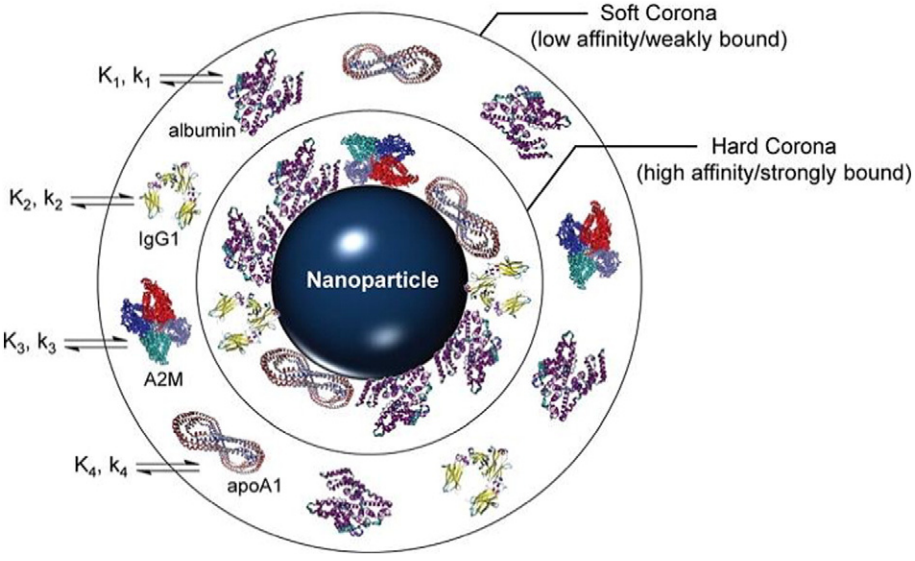

Fig. 3. Schematic of soft and hard corona formed on the surface of a NP. "Protein adsorption is a kinetic (k) and thermodynamic (K) function of both the individual proteins and NP properties such as surface modification, composition, and diameter. Initially, high-abundance and/or high-mobility proteins bind to the nanoparticle surface. Over time, these proteins are replaced by lower-mobility proteins with a higher binding affinity. Serum proteins commonly observed in NP coronas are shown as a representative corona: serum albumin, immunoglobulin G1 (IgG1), alpha-2 macroglobulin (A2M), and apolipoprotein A-1 (apoA1)." Figure and figure legend reproduced from reference [44] under ACS open access policy.

The mathematical equations described indicate that the DLS results depend on few variables including viscosity of solvent [36], instrument [37], temperature [38], RI (refractive index) of the material [39] etc.

2.1.2.3. Particles dispersed in a colloidal system. While the movement of the particles in colloidal dispersion is random and translational, the particles also rotate very fast [40]. The inter-particular interactions are also important as with increasing concentration, the number of collisions within particles increases while the average pathlength traversed by the particles between successive collisions falls [41]. The surfaces of the dispersed particles are altered depending on the adsorbed layer. A common example to this phenomenon is the adsorption of the proteins on the surface of the NPs creating the characteristic *protein corona* [42,43]. The dispersed particles exhibit a hydrated surface wrapped within a cloak of molecules which are not the ingredients of the particles itself. The corona is often found to be composed of 'hard' and 'soft' components (Fig. 3) [44]. The hard corona refers to the inner stable layer tightly bound to the particles [45]. The soft corona is the comparatively loose layer on top of the hard corona composed of molecules of different charges and sizes [46]. In colloidal system what scatters light are these constructs composed of the NP-cores wrapped within the corona of hydrated/solvated surfaces with altered compositions. Therefore, in DLS the particles that are assayed are different in composition and surface chemistry than those originally synthesized.

In a recent study, DLS was successfully employed in order to determine stabilities of PLA (poly-lactic acid) and PMMA (poly-methyl methacrylate) NPs in buffers, simulated biological fluids (saliva, gastric juice, intestinal fluid and lysosomal fluid), serum and tissue homogenates (mice brain, spleen, liver) [47]. While the PLA NPs showed reasonable stability in such biologically relevant conditions, the PMMA NPs were unstable and aggregated over time. Such systematic DLS studies provide with an *in vitro* tool to investigate NPs for stability before *in vivo* studies. In another study Khan *et al.* (2015) [48] have used DLS effectively to investigate the adsorption of proteins e.g., HSA (human serum albumin), BSA (bovine serum albumin) and HB (hemoglobin) on CTAB-stabilized GNPs (gold NPs) of different sizes (2–40 nm). Furthermore, they correlated the data with mathematical modeling in order to deduce the adsorption kinetics and subsequent development of protein corona on GNPs. Additionally, they provided insights on how the structure of protein and surface chemistry of NPs influenced the development of corona. Understanding the dynamics of the growth of protein corona onto NP-surfaces is important from the perspective of how the NPs behave *in vivo* [49]. Salvati *et al.* (2013) has shown that growth of protein corona on top of transferrin-functionalized silica NPs (~50 nm) eliminated their receptor-targeting capabilities [50]. Hence, detailed investigation to understand the chemistry of protein corona on different NPs will enhance their translatory potential and DLS can be an effective tool in such studies along with techniques like ITC (isothermal titration calorimetry), FT-IR (Fourier-transform infrared spectroscopy) and fluorescence spectroscopy.

2.1.2.4. R_H (hydrodynamic radius) and R_g (radius of gyration). The R_H (hydrodynamic radius) is the radius of the hypothetical hard sphere that diffuses with the same speed as the particles assayed under DLS [51]. Hence, R_H is a hypothetical measurement as such hard spheres rarely exist in colloidal dispersions. In reality the dispersed particles are hydrated/solvated which along with its corona are often not spherical. The composition of the corona – especially the soft corona – is dynamic and fluctuates over time depending on the ionic strength, types of smaller and bigger molecules present in the environment and nature of solvents [52,53]. Therefore, DLS provides only an indicative size of the colloid. The R_g (*radius of gyration*) is the mass average distance from the center of mass to every atom within the molecule (e.g., protein) or NP. For smaller NPs exhibiting Rayleigh scattering the R_g is measured by SAXS (small angle X-ray scattering) [54] while static light scattering (SLS) is used for bigger particles showing anisotropic Mie scattering

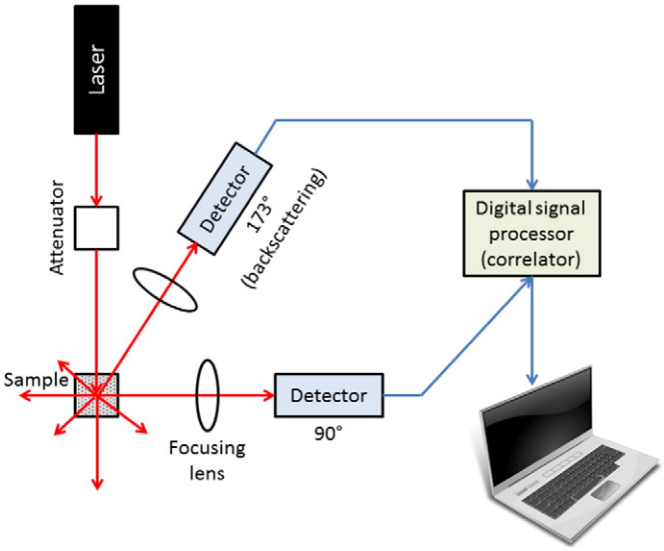

Fig. 4. Schematic showing the instrumentation of DLS.

[55]. The R_g/R_H ratio provides insights into the compactness and shape of the dispersed particles (~0.78 for spherical NPs, 1.5–2.1 for coils and >2 for nanotubes) [56,57].

2.2. Instrumentation and technical aspects of DLS

A range of light scattering instruments [e.g., Malvern (Zetasizer® series), Brookhaven (NanoDLS® series), Microtrac (Wave II® series)] have appeared in recent years. The Malvern Zetasizer® series of instruments are widely popular within university graduates and has emerged as gradual evolution of the original Malvern Correlator® marketed in 1970. Overall these instruments have three major components – laser, sample and light detector (Fig. 4).

2.2.1. Laser

The laser used in Malvern Zetasizers® is 4 mW He—Ne laser of 633 nm wavelength with exceptions of Zetasizer® APS and Zetasizer® μV where 60 mW diode lasers (830 nm) [58] are used. Malvern also supplies DLS instruments with other wavelengths e.g., 532 nm (green). The NanoDLS® series carries laser of 638 nm wavelength [59]. The laser sources provide with a stable beam of coherent monochromatic light. There is an attenuator available to alter the power of laser.

2.2.2. Sample

Clean and square cuvettes made of scratch-free glass or optically translucent disposable plastic (3 × 3 mm, 5 × 5 mm or 10 × 10 mm) are used. Plastic cuvettes with inbuilt electrodes capable of both DLS and ZP measurements (DTS1070 compatible with Zetasizer® ZS, Z and ZS90) are also available. The sample should be clean, homogeneous and transparent without any precipitation. The minimal volume of sample required varies with the model (12 μl for Zetasizer® S, 2 μl for Zetasizer® μV). However, at least 1–2 ml of sample should be prepared in order to obtain good quality data.

2.2.3. Detector

Modern DLS instruments are equipped with APD (avalanche photo diode) detectors which have ~65% quantum efficiency in red wavelengths and thus, lasers of 633 nm are used. In latest instruments the detectors are placed at 173° angle to detect backscattering although in some older versions (Nano S90, ZS90) the angle is still 90°. Placing detectors at 173° enables detection of backscattering and excludes excess scattered light. This helps to unmask scattered light signals of low

intensity originating from smaller particles. It also increases (~8 folds) the area of the illuminated sample within cuvette compared to 90° arrangement [60]. In such NIBS (non-invasive backscatter system) arrangements focusing lens is available to alter the path length of the scattered light before reaching the detector by selecting the illuminated area of the sample to be either in the middle (for dilute samples) or close to the wall (for highly concentrated samples) of the cuvettes, if necessary.

2.2.4. Operating software interface

The current softwares (e.g., Zetasizer®) provide users with possibility to design custom SOPs (standard operating protocols) by offering a series of options. The interface allows the user to insert data for both solvents (e.g., solvent name, viscosity) and the materials (e.g., RI, absorption). The data for most commonly used dispersants (e.g., water, toluene) and materials (e.g., polystyrene, protein) are present by default in the latest versions while online resources are available [61] for details on other solvents and materials. This information becomes particularly important during anisotropic Mie scattering. Inputs on experimental conditions (e.g., temperature, equilibration time) are also required. Once generated, the SOPs can then be run on further samples without modifications. The Zetasizer® shows the size distribution data in the main tab while the second tab shows the ACF (G1(π)–1) and the intensity of fluctuating scattered light (kcps) over time. The third tab is mostly for guidance which systematically tabulates all currently running experiments and shows the quality of data. Upon completion of experiments the data are stored in the retrievable database. Typically, both *z*-average size and size distribution with PDI (polydispersity index) over intensity, volume and number are provided. The size distribution data is available both as line plots or histograms and can be exported with softwares freely available to download from Malvern's online resources.

2.2.5. Data fitting algorithms and analysis

In DLS the ACF of the scattered light is fitted with two different mathematical algorithms:

a) In cumulant method the initial part (up to 10%) of the ACF is fitted into a single exponential decay where the first and the second cumulant term provide with the *z*-average size and PDI, respectively [62]. Therefore, z-average size always provides with single value for every sample. The cumulant method is less vulnerable to noise than other algorithms. However, it is unsuitable for heterogeneous polydisperse samples and in cases may be misleading (Suppl. Material 1).
b) CONTIN algorithm is preferred for polydisperse and heterogeneous samples where cumulant fitting is unsuitable [63]. Here, the correlation function is fitted against longer periods of time and provides size distribution analysis with average size and width for every peak.

For perfectly monodisperse samples both these algorithms should produce same results. However, in reality samples are rarely monodisperse and hence, the results obtained through these two algorithms differ. The PDI for DLS typically depicts the intensity of light scattered by various fractions of the particles differing in their sizes and is calculated by $(\text{width/mean})^2$ for each peak. While PDI of ≤0.1 is considered to be highly monodisperse values of 0.1–0.4 and >0.4 are considered to be moderately and highly polydisperse, respectively.

2.3. Factors that influence DLS results

2.3.1. Sample preparation

Sample preparation is crucial in DLS measurements. The samples are prepared either in solvents (e.g., water, methanol, ethanol, toluene) [64] or diluents (e.g., 10% methanol in water) [65]. Some solvents (e.g., toluene) scatter light [66] which interferes as background noise while some (e.g., DMSO) shows considerable changes in viscosity with variation in temperature [67]. The samples for DLS measurements should be clear, homogeneous and without haze. Checking the bottom of the cuvette for precipitation is useful. Any precipitation confirms the presence of bigger particles which can be due to poor dispersion, wrong pH, inadequate sonication and compromises the experiment. Using DI (deionized) water is usually not recommended as the absence of ions fails to shield the long-distance interactions between particles. Hence, the size obtained in DI water is always 2–10 nm larger than actual size [68]. In few circumstances (e.g., PEC) using dilute saline water gives better data as the ions shield the particles from long-distance interactions. Using 10 mM KNO_3 is better compared to NaCl as chloride ions are highly reactive. Filtering samples to exclude dust particles or lumps is helpful although can produce artificial narrow size distribution. Using properly washed filters of pore sizes three times bigger than (e.g., 5 μm) the expected largest particles within samples can be done. Large particles of low density may float on top of the solvent layer (*creaming*) [69] and can render DLS ineffective. For powder formulations (e.g., freeze dried products) stirring vigorously can dissolve the NPs. Sonication deserves caution especially when proteins are involved. For polymeric NPs it can take up to 24 h by sonication to obtain a stable and homogeneous dispersion.

2.3.2. Sample concentration

Higher concentration of NPs results in multi-scattering where the scattered light from one particle interacts with other particles before reaching detector and loses intensity [70]. As a result the obtained size is artificially smaller. Unpredictable agglomeration happens in high concentrations unless surfactants are used [71]. On the contrary, using too dilute samples may not generate enough scattered light to analyze. Therefore, finding optimal sample concentration is essential. It is difficult to provide a general guideline on the ideal concentration for DLS as it varies and depends upon factors related to both the instrument (e.g., scattering volume, angle of scattering, laser power, detector sensitivity) [72] and material properties (e.g., molecular weight, compactness) [73] of the particles. For example, NPs that are spherical and more compact scatter more light than NPs that are less compact [74]. The Malvern Zetasizer® manual states that at least one million (10^6) residual photons should be detected during the experiment to acquire good quality data with high signal-to-noise (S/N) ratio where residual photons mean the difference between scattered photons from the sample and solvent. The user manual of Brookhaven Instruments suggests a sample concentration able to generate counts maximum up to 600 kcps although counts within 500–600 kcps work fine for most samples. The noise in DLS experiments varies inversely proportional to the square root of photons counted and hence, there is a minimal threshold for photon counts required to achieve good S/N ratio. In practice, it may be necessary to run DLS experiments on serial dilutions to determine the optimal concentration.

2.3.3. Colored and fluorescent samples

Ideally colored and fluorescent samples should be avoided in DLS [75]. The use of fluorescent NPs has increased as they are often coupled with microscopy. It is essential to run control experiments to exclude the possibility of absorption of light by the fluorophores at the wavelength of laser. In case of absorption, the intensity of the scattered light will be lower and hence, artificial smaller size for the particles will be estimated [76]. Fluorescent light is non-coherent and recorded as noise. The APD detectors are often not capable to differentiate between various intensities. As a result in case of fluorescence there can be heightened noise which deteriorates S/N ratio resulting in low quality data and broadening of peaks. Unfortunately, a lot of the popular fluorophores absorb and emit within 600–700 nm which interferes with DLS. To minimize such interferences, in some instruments a narrow band filter to screen out wavelengths different from the laser

(e.g., 633 ± 2.5 nm) is present. However, it also reduces the number of photons detected and hence, higher concentrations may be required.

2.3.4. Effect of agglomeration

NPs tend to agglomerate [77] and while some of these agglomerations are reversible, often it is not the case. Therefore, different surfactants are frequently used to produce stable dispersions [78]. It is difficult to obtain high quality data from dispersions with agglomerated NPs as the bigger agglomerated lumps scatter too much light which may damage the detector. Excessive scattering also masks low intensity scattered light from smaller particles. Hence, broadened peaks emerge while confidence in the data is reduced. Agglomeration is enhanced by increasing concentrations and thus, DLS is reliable only at dilute concentrations (typically 50–100 μg/ml) which makes it unsuitable for many therapeutic formulations where much higher (up to few mg/ml) concentrations are used [79].

2.3.5. Shape of NPs

Often NPs are not spherical e.g., nanostars [80], nanotubes [81]. For such NPs the DLS provide a R_H which by definition is the radius of a hypothetical hard sphere moving at the same speed to that of the aspherical NPs within dispersion. In a recent paper Nair *et al.* [82] have modified the *Stokes-Einstein* equation to fit the data obtained from cylindrical structures (e.g., nanotubes):

$$D_t = \frac{k_B T}{3\pi\eta L}\left[\ln\left(\frac{L}{d}\right) + 0.32\right] \quad (6)$$

Where k_B = Boltzmann constant ($1.38064852 \times 10^{-23}$ J/K), T = temperature, η = absolute viscosity, L = length of cylinder and d = diameter of cylinder. The aspect ratio (L/d) is known for nanotubes and hence, the D_t for such cylindrical nanomaterials can also be determined by DLS.

2.3.6. Rotational diffusion of NPs

In DLS typically the translational diffusion coefficient (D_t) is determined while the rotational diffusion coefficient (D_r) often goes undetected as the dispersed particles rotate extremely fast. However, for some particles (e.g., colloidal gold, larger and crystalline NPs) intensity peaks at smaller sizes (0-10 nm) may appear due to rotational diffusion of particles [83]. The easiest way to identify these peaks is to compare the DLS spectra on the same sample at 90° and 173° scattering angles. Unlike translational diffusion the scattering of light due to rotation of particles is not angle-dependent and hence, no shift for peaks due to rotational diffusion will be observed. On the contrary peaks due to translational diffusion shift at different scattering angles.

2.3.7. Issues related to cuvette

Plastic cuvettes should be avoided for samples with organic solvents or experiments requiring temperature of ≥50 °C. Especially for glass cuvettes, when the area of illumination is close to its wall – a part of the reflected laser from the wall may be recorded by the detector as high intensity light. This is known as *flaring* and typically shows up as sharp peak at 1–10 μm. To avoid flaring the area of illumination should be moved towards the middle of the cuvette using the focusing lens.

2.3.8. Maintenance of the instrument

Proper maintenance of the instrument is required to obtain consistent high quality data from DLS. The instrument should be left undisturbed for at least 30 min after switching it on to give sufficient time for the laser to stabilize. As per the guidelines published by the NIST (National Institute of Standards and Technology) [84], the instruments should be regularly checked with reference NPs with precisely known size and very low PDI. Cytochrome C or BSA (bovine serum albumin) and latex beads of different sizes (e.g., 100 nm) can be used as references for sizes ≤20 nm and ≥20 nm, respectively. The instrument should be able to show sizes within 2% deviation for reference samples. Colloidal gold of different sizes can also be used as reference material.

2.4. Practicalities

2.4.1. Resolution of DLS

An inherent weakness of DLS is its low resolution [85]. For example, DLS is unable to distinguish between particles of 90 and 110 nm and a broad peak with high PDI will appear. In order to offer peak resolution, DLS requires particles different in size by at least a factor of 3 (e.g., 10 and 30 nm, 50 and 150 nm) [86]. This is a limitation of DLS especially for polydisperse samples. To increase resolution prior size-separation of particles can be done [87]. Latest DLS instruments can be coupled with analytical instruments which enable DLS to determine size of every fraction precisely.

2.4.2. Expressing the R_H based on intensity, volume or number

A common dilemma faced by researchers is how to express the particle size as most of the current DLS softwares offer options to express particle size distribution based on intensity, number and volume. Expressing the data on these three parameters often produce three different R_H and size distributions. The principles of DLS are based on measuring intensity of scattered light and hence, the representative R_H value should always be deduced on intensity measurements while the other two parameters (volume and number) should be used as supporting information only.

2.4.3. Importance of feeding right information to the software

Softwares like Zetasizer® needs to be fed with data regarding both the dispersant (e.g., RI, viscosity) and dispersed (e.g., RI, absorption) phases. For Rayleigh scatterers (≤100 nm) this information is often not required. However, for particles >100 nm – which is often the case for nanoparticulate DDS – this information becomes crucial. Knowing the accurate RI and viscosity of the sample is essential in such cases and can be obtained by use of refractometer and rheometer, respectively. It is difficult to predict how NPs alter the viscosity of the sample. As a working guideline it can be stated that if the number of NPs per unit volume of dispersant increases with increasing concentration then it usually also increases the viscosity of the dispersion [88]. It is crucial to know these parameters about the dispersant and instruct the software accordingly to avoid erroneous data. An example where DLS was run on a dispersion of stable and highly monodisperse carboxylated latex beads (~100 nm) in water (100 μg/ml) at 25 °C but analyzed on set ups for different dispersants (40% sucrose, water, methanol and toluene) is shown in Fig. 5. It is surprising that the z-average size of the particles in the same sample varied drastically from ~15 nm (40% sucrose) to ~155 nm (toluene) showing how dependent DLS data are on these inputs.

2.4.4. Proper reporting of DLS data

The NIST has issued the following instructions on reporting DLS data [84]:

> "*At a minimum, the mean z-average diameter (or radius) and mean polydispersity index should be reported, along with their standard deviations based on at 3 to 10 replicate measurements. The number of replicate measurements should also be reported. If a size distribution analysis algorithm is applied, then it should be identified along with any key parameter values used in the analysis. Other critical information that should be reported includes: particle concentration (mass or volume based), dispersion medium composition, refractive index values for the particles and the dispersion medium, viscosity value for the medium, measurement temperature, filtration or other procedure used to remove extraneous particulates/dust prior to analysis (including pore size and filter type), cuvette type and size (pathlength), instrument make and model, scattering angle(s), and laser wavelength. Additional*

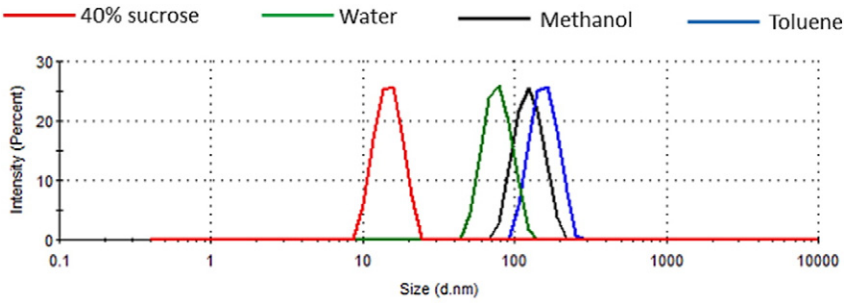

Solvent	Viscosity (cP)	RI	z-average (nm)	PDI
40% sucrose	5.1178	1.4	15	0.008
water	0.8872	1.33	87	0.009
methanol	0.5476	1.326	122	0.011
toluene	0.5564	1.496	153	0.005

Fig. 5. Intensity-based DLS data on same 100 μg/ml dispersion of commercially available carboxylated latex beads (~100 nm mean size) in water at 25 °C with Zetasizer® software while set ups with four solvents with different viscosities and RI (40% sucrose, water, methanol and toluene) were chosen. The z-average size varied from 15 nm to 153 nm depending on the solvent.

information that can be helpful to include in a report: *measured auto-correlation y-intercept* (*amplitude*), *mean count rate during measurements*, *duration of a single measurement*, *and mean signal-to-noise ratio*."

Therefore, extensive information on how the DLS measurements were done needs to be provided to ensure both quality and reproducibility. Unfortunately, the DLS data reported in drug delivery literature rarely meets such high standards and this issue needs to be addressed urgently.

2.4.5. Comparison of DLS with other techniques to measure particle size

2.4.5.1. TEM (transmission electron microscopy). Different formats of EM (electron microscopy) [89] e.g., TEM [90] are quite popular for imaging NPs. With image analysis softwares (e.g., ImageJ®) it is now possible to obtain size distributions of NPs from TEM images with information on mean size, standard deviation and overall estimation of PDI. However, such information from TEM images often do not corroborate well with data obtained from DLS as the latter is an intensity-based technique [91] whereas TEM is a number-based one [92] making them fundamentally different. While the samples for DLS are solvated, TEM works on dry samples under UHV (ultrahigh vacuum) conditions [93]. DLS measures the R_H of the dispersed particles whereas TEM provides the projected surface area based on how much of the incident electrons were transmitted through the sample. Hence, the size obtained by DLS is usually bigger than TEM. An advantage with DLS is its capability to measure bigger number of particles (in millions) compared to TEM (few hundreds). Therefore, DLS provides more robust data on size distribution and PDI.

2.4.5.2. NTA® (nanoparticle tracking analysis). With the launch of Nanosight® series of instruments from Malvern the use of NTA® software has increased rapidly for determining particle size [94]. Both these techniques determine particle size from the D_t (Section 2.1.2.2 of this review) with *Stokes-Einstein* equation. However, the way they determine the D_t is different and hence, the sizes obtained by these two techniques are often not same. While NTA® detects the D_t by recording the mobility of the NPs from scattered light captured as videos through CCD cameras, DLS detects it by correlating the fluctuation in intensity of the scattered light over time. To compare these two techniques the following points are made [39]: (i) The particle density within samples required for DLS (10^8–10^{12}/ml) is usually higher than NTA® (10^7–10^9/ml); (ii) For same sample usually the size obtained from DLS is smaller but with more error compared to NTA®; (iii) NTA® is more effective than DLS in analyzing polydisperse samples. The data analysis report in NTA® plots the sizes of the particles on 3D space compared to the 2D report in DLS. As a result, NTA® offers better resolution and is less vulnerable than DLS to be influenced by high intensity scattering from bigger particles; (iv) While both techniques are capable in analyzing submicron particles, DLS is more capable to detect sizes <30 nm. Overall NTA® offers better analytical suite for therapeutic nanoformulations dealing especially with peptides and macromolecules. However, it lacks the simplicity of DLS, is more expensive, requires extensive sample preparation and training.

2.4.5.3. AFM (atomic force microscopy). AFM has emerged as an effective tool to image NPs especially due to its ability to work on biological samples rich in water [95,96]. AFM provides precise information on particle size and shape while also able to recognize particles of different sizes in a mixture. However, the number of particles analyzed by AFM is much smaller and thus DLS provides better size distribution and PDI.

2.4.5.4. Particle size determination by sedimentation (X-ray disc centrifuge and DCS/differential centrifugal sedimentation). Recently, determination of NP size based on sedimentation technique has gained popularity (e.g., encapsulated drugs, viruses, liposomes, emulsions), although the principles of such techniques were already known before. A detailed discussion and in-depth analysis of these techniques fall out of the scope for this review although excellent literature material and technical notes are available [97–99]. In short, these techniques utilize high centrifugal force to deposit NPs in fractions based on density. The sizing of the NPs is done by monitoring the deposition of the particles on a rotating disc either by X-ray absorbance (X-ray disc centrifuge) or monochromatic light λ = 400–500 nm (DCS). The mathematical operator for these techniques is the *Stoke's law* (Eq. (7)):

$$V = \frac{d^2 g\left(\rho_p - \rho_f\right)}{18\eta} \tag{7}$$

where V = velocity (settling rate), d = diameter of particle (cm), g = gravitation acceleration (981 cm/s^2), ρ_p = particle density (g/ml), ρ_f = fluid/dispersant density (g/ml), η = viscosity (poise).

Such particle sizing based on sedimentation techniques offer certain advantages over DLS: (i) They yield accurate and highly reproducible data with excellent (~2%) peak resolution which is not achievable with DLS; (ii) These tools can operate on particles with a very broad size range (2 nm–80 μm) whereas the operational size-detection window for DLS is only 10–200 nm; (iii) The sizes of particles measured with these techniques are comparable to SEM/TEM data whereas for DLS it is almost always bigger than SEM/TEM; (iv) These techniques offer multi-modal size determination with high-throughput modes where ~40 samples of 100 μl volume each can be run simultaneously.

It is crucial to realize that the sedimentation techniques determine size of NPs based on their density. Hence, DCS is unable to differentiate between two different NPs as long as their density is same. For example, DCS may yield same size for smaller solid and larger porous particles from same material given the particles are of same density. DCS also may be difficult to perform for non-spherical particles and usually provides smaller size (*Stoke's equivalent*) than actual measurements. For example, rods with aspect ratios of 2 and 3 are known to generate sizes which are 5% and 10% lesser than actual measurements, respectively. DCS is difficult for particles with density lower than the dispersant as they tend to float. However, with current instrumental advancements such challenges are usually resolved. DCS however requires bigger sample volumes (100 μl) whereas modern DLS instruments can operate on as low as 12 μl. Additionally, with current compact instruments like Malvern Zetasizer® both particle (hydrodynamic) size and zeta potential can be measured while DLS which is not possible in DCS.

2.4.5.5. Particle size determination by laser diffraction. Laser diffraction is a capable tool to determine the size of NPs and its core principles, like DLS, are also based on scattering of light [100]. Particles scatter light in a size-dependent way where bigger particles scatter more intensely at smaller angles and smaller particles scatter with lesser intensity at wider angles. In laser diffraction technique, the scattering of light is expressed as a function of scattering angle which in turn is used to measure particle size.

The main differences with DLS are: (i) Laser diffraction technique determines the size of a particle which scatters light in a similar way to that of the particles under investigation. On the contrary, DLS measures the (hydrodynamic) radius of a hypothetical solid particle scattering light with same intensity as the particles under investigation while diffusing in the dispersion. Therefore, the results obtained through these techniques are not same and often differ by 10–20% depending on the experimental conditions and type of NPs; (ii) The lower limit of detection is smaller for DLS whereas the upper limit of detection is bigger in laser diffraction. Therefore, for smaller NPs (e.g., ≤50 nm) DLS provides better data whereas for bigger particles (e.g., ≥1 μm) laser diffraction is more suitable; (iii) Much lesser volume of sample is required for DLS (in μl) whereas bigger volumes are required for laser diffraction (in ml); (iv) Laser diffraction is more suitable in samples with particulate impurities of larger sizes. Overall laser diffraction offer a better sizing tool for nanoformulations meant for drug delivery as they are often ≥100 nm. However, it does not offer the compact size and zeta potential determining experimental suite and hence, the simplicity of DLS is absent with laser diffraction technique.

2.4.6. DLS in cell culture medium

Performing DLS in cell culture medium (e.g. DMEM, RPMI) can be difficult as they contain a wide range of smaller (e.g., ions) and larger (e.g., vitamins) molecules. As a result of adsorption of these molecules, the surface properties and the sizes of the NPs change. This becomes particularly evident for medium containing FCS (fetal calf serum) enriched with proteins. Adsorption of larger protein molecules can show drastic and rapid increase of R_H for the dispersed NPs [101,102]. The adsorbed layers on NPs are dynamic in composition and hence, the R_H fluctuates over time before stabilizing. Cell culture medium without pH indicators (e.g., phenol red) should be used as the colored material can absorb the laser and interfere.

2.4.7. DLS on aerosols and foams

Newer colloid formulations e.g., aerosols, foams are becoming popular in drug delivery. It is difficult to perform DLS measurements on such samples and SMPS (scanning mobility particle sizer) is the technique of choice for such preparations. However, there are reports available in literature where DLS was used to measure particle size for aerosols and foams. As example [103], the size of aerosolized carbon soot originating from burning cigarette tips was measured in a custom-built light scattering instrument at 90° scattering angle. Similar attempts were made by Durian *et al.* (1991) where light scattering technique was used to ascertain particle size as well as internal dynamics of foams [104].

3. Zeta potential (ZP)

3.1. Principles of ZP

The ZP, also termed as *electrokinetic potential*, is the potential at the slipping/shear plane of a colloid particle moving under electric field [105]. Electric potential of a surface is the amount of work that needs to be done to bring a unit positive charge from infinity to the surface without any acceleration. The ZP reflects the potential difference between the EDL (electric double layer) of electrophoretically mobile particles and the layer of dispersant around them at the slipping plane.

3.1.1. Understanding the EDL and slipping plane

When a charged particle is dispersed, an adsorbed double layer – often referred as EDL [106] - develops on its surface (Fig. 6). The inner layer consists predominantly of ions/molecules with opposite charge to that of the particle (*Stern layer*). Beyond Stern layer the electrostatic effects due to the surface charge on the particles decrease as per *Debye's law* - which states that with the distance of each Debye length the field decreases by a factor of 1/e [107].

Although mathematically this electrostatic effect extends till infinity, experimentally it is only present till few nm from particle surface. Due to the electrostatic field of the charged NPs, a diffuse layer consisting of both same and opposite charged ions/molecules grow beyond the Stern layer which along with the Stern layer forms the EDL. The composition of this diffuse layer is dynamic and varies depending on a variety of factors e.g., pH, ionic strength, concentration etc. When an electric field is applied to such dispersion, the charged particles move towards the opposite electrode (*electrophoresis*). Within this diffuse layer there is a hypothetical plane which acts as the interface between the moving particles and the layer of dispersant around it while electrophoresis. This plane is the characteristic *slipping/shear* plane and ZP is the potential at this particle-fluid interface. Greek letter ζ (zeta) was used originally in mathematical equations while describing it and hence, the name zeta potential. The potential on the particle surface itself is known as the *Nernst potential* (ψ_0) [108] and cannot be measured. The electrostatic field decreases in dispersion with distance from the particle surface as per Eq. (8):

$$\psi = \psi_d e^{-\kappa x} \tag{8}$$

where ψ = surface potential at distance x from the stern layer, ψ_d = surface potential at stern layer, κ = Debye-Hückel parameter, x = distance.

When the slipping plane is in close proximity to the stern layer - the $\psi_d \approx \zeta$ and hence, Eq. (8) can be modified as Eq. (9):

$$\psi = \zeta e^{-\kappa x} \tag{9}$$

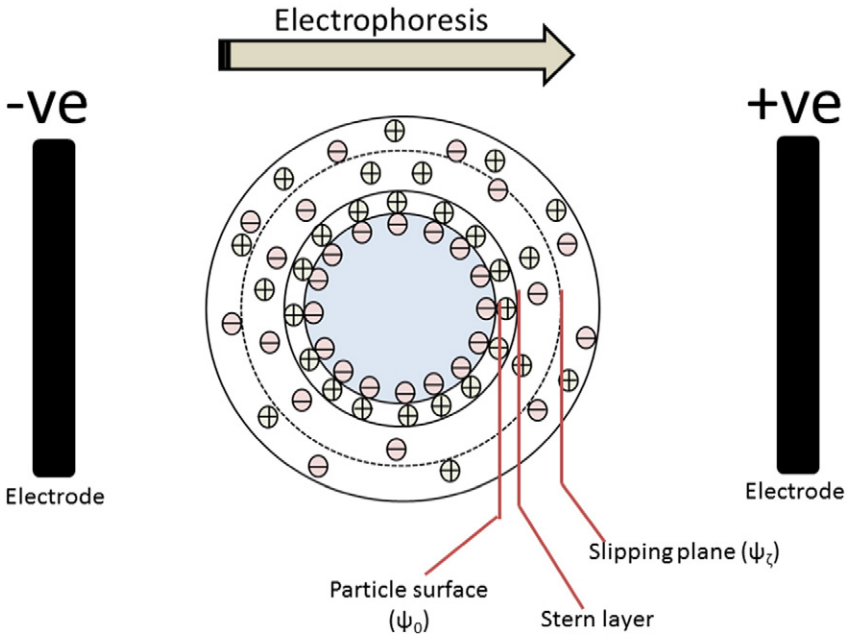

Fig. 6. Cartoon showing the EDL on a negatively charged particle. Immediately on top of the particle surface there is a strongly adhered layer (Stern layer) comprising of ions of opposite charge i.e. positive ions in this case. Beyond Stern layer a diffuse layer develops consisting of both negative and positive charges. During electrophoresis the particle with adsorbed EDL moves towards the electrodes (positive electrode in this case) with the slipping plane becoming the interface between the mobile particles and dispersant. The ZP is the electrokinetic potential at this slipping plane.

The κ (Debye-Hückel parameter) depends on the ionic strength. Hence, with increased ionic presence (e.g., addition of electrolytes) the double layer gets compressed and the ZP decreases.

3.1.2. Fundamental mathematical operators while measuring ZP

ZP cannot be measured directly and is deduced from electrophoretic mobility of charged particles under an applied electric field. The electrophoretic mobility (μ_e) of the particles is first calculated as (Eq. (10)):

$$\mu_e = \frac{V}{E} \tag{10}$$

where V = particle velocity (μm/s), E = electric field strength (Volt/cm) – both known quantities. The ZP is then calculated from the obtained μ_e by the *Henry's equation* (Eq. (11)):

$$\mu_e = \frac{2\varepsilon_r\varepsilon_0\zeta f(Ka)}{3\eta} \tag{11}$$

where ε_r = relative permittivity/dielectric constant, ε_0 = permittivity of vacuum, ζ = ZP, $f(Ka)$ = Henry's function and η = viscosity at experimental temperature.

When the thickness of the EDL is much smaller compared to the particle radius - which can be due to bigger particles (up to 1 μm) within aqueous solutions of high salt concentration (10^{-2} M) - the value of $f(Ka)$ is taken as 1.5 and the Henry's equation then modifies into the *Helmholtz-Smoluchowski* (*HS*) equation (Eq. (12)):

$$\mu_e = \frac{\varepsilon_r\varepsilon_0\zeta}{\eta} \tag{12}$$

The HS equation applies to most of the pharmaceutical preparations and hence, very important for developing nano-DDS [109].

On the contrary when the thickness of EDL is much bigger than the particle itself due to smaller (≤100 nm) particles dispersed in low salt concentration (10^{-5} M) the value of $f(Ka)$ is taken as 1 and the Henry's equation can be modified as the *Hückel equation* (Eq. (13)):

$$\mu_e = \frac{2\varepsilon_r\varepsilon_0\zeta}{3\eta} \tag{13}$$

The Hückel equation is usually not relevant for pharmaceutical preparations as it is not applicable for aqueous dispersions although it is popular in ceramic industry.

3.2. Instrumentation in ZP measurements

An electric field is applied and the electrophoretic mobility of the particles is measured in the following two ways:

a) *Electrophoretic light scattering*: The mobile particles during electrophoresis scatter an incident laser. As the particles are mobile the scattered light has different frequency than the original laser and the frequency shift is proportional to the speed of the particles (Doppler shift). The instrumentation used for this technique is shown in Fig. 7. In short the laser beam is split into two and while one beam is directed towards the sample the other one is used as reference beam. The scattered light from the sample is combined or *optically mixed* with the reference beam to determine the Doppler shift. The magnitude of particle velocity (V) is deduced from the Doppler shift and then the ZP is measured through the series of mathematical equations enlisted as Eqs. (10)–(13). This technique is often used in conjunction with DLS and hence, a range of instruments (e.g., Malvern Zetasizer®) providing integrated measurement suite for both DLS and ZP have emerged which are popular within university graduates and nanoformulation groups. The Zetasizer® series of instruments use sophisticated laser interferometric M3-PALS (phase analysis light scattering) technique [110] for such applications. Disposable plastic (polycarbonate) cuvettes with inbuilt gold plated copper electrodes and bent capillary tube to hold 0.75 ml of sample are available to conduct both DLS and ZP measurements at a single run. Like DLS the Zetasizer® software interface allows the user to develop customized SOPs and insert relevant information.

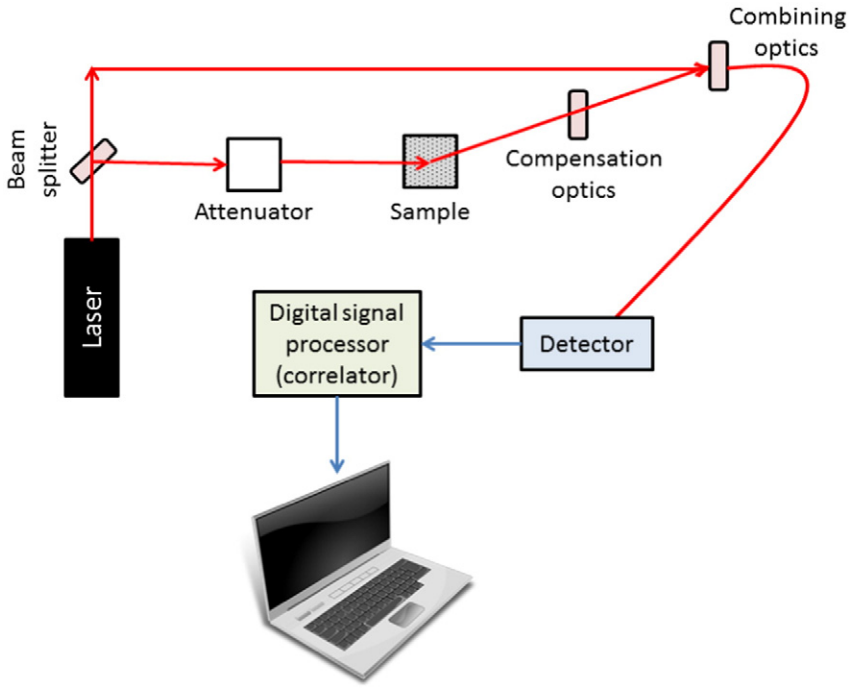

Fig. 7. Schematic showing the instrumentation of ZP measurement by electrophoretic light scattering.

b) *Electroacoustic phenomenon*: In this technique an electric field of high frequency is applied which makes the particles in sample oscillate while the oscillation depends on their size and ZP. The oscillation is analyzed on magnitude and phase angle to determine both the particle size and ZP [111]. This technique is less popular in drug delivery research.

3.3. Interpretation of ZP data

3.3.1. Factors influencing ZP

3.3.1.1. pH. pH is perhaps the most influential parameter in ZP measurements especially in aqueous dispersions which makes it relevant for pharmaceutical formulations. The ZP varies with pH and becomes more positive and negative in magnitude with acidic and basic pH, respectively [112]. Therefore, a titration curve of ZP against different pH values is often generated which helps to determine the isoelectric point i.e. the pH where the ZP becomes zero [113]. For aqueous dispersions - where H^+ and OH^- are major ionic constituents - the isoelectric point also denotes the PZC (*point of zero charge*) [114]. Colloids lose stability and agglomerate/flocculate when the pH is close to the isoelectric point.

3.3.1.2. Ionic strength. With increasing ionic strength the EDL becomes more compressed while the ZP decreases and vice versa. The valency of the ions is also important while measuring ZP. For ions with higher valency (e.g., Ca^{2+}, Al^{3+} having higher valency than monovalent Na^+, H^+, OH^-) the EDL becomes more compact and the ZP decreases in magnitude.

3.3.1.3. Concentration. The relation between ZP and particle concentration is complex and usually determined by both surface adsorption and the effect of EDL. It is difficult to provide with a general guideline on effect of concentration on ZP. However, it can be stated that overall in dilute conditions the surface adsorption phenomenon dominates and hence, the ZP increases with concentration. However, at higher concentration range the thickness of EDL dominates and then by increasing concentration an opposite effect i.e. decrease in ZP with lesser stability of the dispersion is observed [115].

3.3.2. ZP and colloid stability

One of the most popular uses of ZP data is to relate it with colloid stability. Guidelines classifying NP-dispersions with ZP values of ±0–10 mV, ±10–20 mV and ±20–30 mV and > ± 30 mV as highly unstable, relatively stable, moderately stable and highly stable, respectively are common in drug delivery literature [116]. Unfortunately, the reality is more complex than that. Although ZP does provide indications on colloid stability it does not reflect the entire picture. As per the most widely accepted DLVO (named after inventors Derjaguin, Landau, Verwey and Overbeek) theory colloid stability depends on the sum of van der Waals attractive forces and electrostatic repulsive forces due to the EDL [117]. While ZP provides information on the electrostatic repulsive forces it does not provide any insight on the attractive van der Waals forces. Therefore, it is not uncommon to come across stable colloids with low ZP and vice versa. There is plenty of theory involved in understanding such attractive forces in nature like van der Waals which falls beyond the scope of this review. One important point to note is that the van der Waals attractive force is dependent on the *Hamaker constant* [118] which indirectly corresponds to the difference between the RI of the particle and the dispersant. Therefore, if the Hamaker constant is low the van der Waals attractive forces also become weak and then mild electrostatic repulsion reflected by low ZP (e.g. 10–15 mV) may be enough to ensure colloid stability. Materials like colloidal silica shows exceptional stability at very low ZP [119]. It should be noted that steric interactions can also contribute to colloid stability. For example some water-in-oil emulsions are highly stable despite having low ZP [120]. PEGylation is also known to facilitate stability of NPs while decreasing the ZP [121].

3.3.3. ZP and surface charge of NPs

Another widely popular use of ZP is to use it in assessing the surface charge of NPs. The positive or negative dimensions of ZP are determined by identifying which electrode the particles are moving towards during electrophoresis. It should be noted that ZP never measures charge or

charge density and rather deals with surface potential. Therefore, only the magnitude of ZP is important while the positive/negative finding associated with it is not robust and should not be related with surface charge or charge density or making comparisons between different nanoformulations. As stated in previous sections of this review, a wide variety of factors (e.g., pH which is relevant for nanoformulations) can change it from +ve to –ve and vice versa. ZP only provides with indicative evidence towards the nature of surface charge (positive/negative) assuming that the predominant ions in the EDL up to the slipping plane are similar (positive/negative) compared to the surface of the particle itself. Unfortunately, there are too many exceptions to such assumption. The practical way to confirm the nature (positive/negative) as well as to determine charge density on NPs is to titrate it with known amounts of ions. A detailed description of such titration technique falls beyond the scope of this article although excellent reference literature is available [122,123].

Charge on particle-dispersant interface (e.g., slipping plane) is a complicated and less understood phenomenon. Usually, almost all of the naturally occurring surfaces and molecules exhibit negative charge (e.g., cell membrane, proteins, lipids, mucus etc.). On the contrary cationic surfaces and molecules are often synthetic. It is also inappropriate to claim having "neutral" NPs based on ZP as there are never neutral NPs in dispersion due to inevitable charge build up on their surfaces. An interesting fact is that surface charge on NPs can actually vary depending on the different phases within the colloid. As per Cohen's rule if both solute and solvent are insulators then the one with higher relative permittivity (ε_r) becomes positive at the interface. Hence, in room temperature silica ($\varepsilon_r = 3.9$) NPs are negatively charged in water ($\varepsilon_r = 80$) but positively charged in benzene ($\varepsilon_r = 2.27$).

3.4. Practicalities

3.4.1. Reference materials

Unlike DLS there are as such no reference or standard materials for ZP which is inconvenient in practical terms. The NIST has suggested the use of Goethite (α-FeO(OH)) which upon preparation under specified conditions should deliver a ZP of $+(32.5 \pm 0.12)$ mV [124]. However, the samples need to be made fresh every time and it may foul the cuvette. Slight variation in data based on instruments may also occur.

3.4.2. Reusing samples after measuring ZP

Electrophoresis may degrade some NPs and hence, may render the samples unsuitable for reuse after measuring ZP. As a common guideline it can be stated that if possible reusing samples for experiments after measuring ZP should be avoided. If that is not the case (e.g., due to small volume of sample) then adequate re-characterization of the particles including DLS and gel electrophoresis should be done after measuring ZP to exclude any degradation of the particles under applied voltage.

3.4.3. Using buffers with metallic ions

The electrodes in cells for ZP measurements are prone to react especially with metallic ions (e.g., Fe^{3+}) [125]. Such reactions can destroy the electrode and compromise the quality of data. Therefore, regular checking of the electrode is advisable. In case the contact between the electrodes and the ions cannot be prevented in spite of deleterious reactions then *diffusion barrier method* [126] can be used where the electrophoretic mobility of the particles can still be measured while preventing any contact between electrode and the buffer. However, it requires additional expertise.

3.4.4. Measuring ZP in cell culture medium

It can be challenging to measure ZP in cell culture medium. Enriched with plenty of ions, the cell culture mediums have very high conductivity and interfere with ZP measurements. Such high conductivity can generate enough heat under constant voltage which may degrade the sample. Using higher concentrations of NPs (5–10 mg/ml) under low voltage can be helpful to obtain a stable ZP reading. Unfortunately, it becomes much more complex in cell culture medium carrying FCS which contains plenty of proteins. The available protein molecules get adsorbed on the NP-surfaces and influence both the dispersion and ZP [127]. The protein molecules also sometimes make small nanoagglomerates which interfere with the readings and can generate additional aberrant peaks.

4. Discussion

The fundamental principles of both DLS and ZP are rooted within the realms of physical colloid chemistry and it is essential to have strong grip over the core physical and mathematical principles in order to understand their applied aspects. The basics of DLS and ZP are taught already to the undergraduate students in physical chemistry in most universities. Unfortunately, similar training and structured grooming process for young researchers performing DLS and ZP are often missing in drug delivery research groups. This gap in knowledge as well as lack of proper training needs to be addressed.

Both DLS and ZP measurements are based on light scattering and hence, only clear samples can be subjected to these two techniques. Additionally, both these techniques are not capable to handle concentrated samples. Just to exemplify, the *Stokes-Einstein equation* – which is the backbone of particle size measurements based on light scattering – is only mathematically feasible at infinitely dilute concentrations. In reality usually 50–100 μg/ml concentrations are used. Unfortunately, it hardly correlates with therapeutically relevant doses which are much higher in concentration with particles frequently >200 nm present in it. As a result the prepared nanoformulation samples are often neither clear nor dilute enough to be fit for DLS and ZP measurements. It needs to be emphasized that DLS and ZP have their own shares of limitations and their inability to handle high concentrations is a major weakness of both these techniques. Surface chemistry is important in measuring the DLS and ZP and any change in surfaces of the particles will alter the results. In therapeutically relevant samples with high concentration containing complex engineered nanoconstructs – plenty of parameters (e.g., viscosity, pH, dielectric constant, RI etc.) change and hence, the dilute samples used for DLS and ZP measurements are never an adequate representation of the therapeutic formulations to be used *in vivo*. Hence, results from DLS and ZP should not provide grounds for rushing nanoformulations for *in vivo* studies. The DLS and ZP are run mostly on aqueous dispersants with known ionic strength and pH under controlled laboratory environments that are hardly comparable to *in vivo* circumstances where the dispersion medium often is blood with a complex matrix. The DLS and ZP neither operate in blood nor can predict the behavior of NPs in blood. These two techniques were originally developed for protein dispersions and although they work fine with engineered NPs within certain operational conditions, the scope of them in characterizing nanoformulations *in vivo* is limited.

Unfortunately, at this stage the lack of adequate analytical tools capable to handle complex biological matrices (e.g., blood) is missing and the focus of ongoing research work should try to address this issue urgently in order to facilitate translation. In last few years a wide range of nanoformulations have emerged although their translational impact overall has been disappointing with poor *in vitro – in vivo* correlation [128–130]. There are challenges in characterization of NPs under physiologically relevant conditions. DLS and ZP are excellent tools to characterize NPs at their initial stages of development. However, the scopes for these two techniques become increasingly limited in further phases of nanoformulation preparation or to provide sound data for *in vivo* correlation.

Conflict of interest

The author would like to declare no conflict of interest.

Acknowledgements

Funding and access to scientific literature was provided by UCD. The author would like to thank his colleagues and students for innumerable discussions which laid the foundation of this review. Dr. Dermot Brougham and Dr. Delyan Hristov from UCD School of Chemistry are thanked for stimulating discussions and providing latex beads, respectively.

Appendix A. Supplementary data

Supplementary data to this article can be found online at http://dx.doi.org/10.1016/j.jconrel.2016.06.017.

References

[1] L. Treuel, K.A. Eslahian, D. Docter, T. Lang, R. Zellner, K. Nienhaus, G.U. Nienhaus, R.H. Stauber, M. Maskos, Physicochemical characterization of nanoparticles and their behavior in the biological environment, Phys. Chem. Chem. Phys. 16 (2014) 15053–15067.
[2] A. Akbarzadeh, M. Samiei, S. Davaran, Magnetic nanoparticles: preparation, physical properties, and applications in biomedicine, Nanoscale Res. Lett. 7 (2012) 144.
[3] S. Bhattacharjee, D. Ershov, K. Fytianos, J. van der Gucht, G.M. Alink, I.M. Rietjens, A.T. Marcelis, H. Zuilhof, Cytotoxicity and cellular uptake of tri-block copolymer nanoparticles with different size and surface characteristics, Part. Fibre Toxicol. 9 (2012) 11.
[4] S. Bhattacharjee, L.H. de Haan, N.M. Evers, X. Jiang, A.T. Marcelis, H. Zuilhof, I.M. Rietjens, G.M. Alink, Role of surface charge and oxidative stress in cytotoxicity of organic monolayer-coated silicon nanoparticles towards macrophage NR8383 cells, Part. Fibre Toxicol. 7 (2010) 25.
[5] P.M. Favi, M. Gao, L. Johana Sepúlveda Arango, S.P. Ospina, M. Morales, J.J. Pavon, T.J. Webster, Shape and surface effects on the cytotoxicity of nanoparticles: gold nanospheres versus gold nanostars, J. Biomed. Mater. Res. A 103 (2015) 3449–3462.
[6] J.V. Jokerst, T. Lobovkina, R.N. Zare, S.S. Gambhir, Nanoparticle PEGylation for imaging and therapy, Nanomedicine (London) 6 (2011) 715–728.
[7] B. Kong, J.H. Seog, L.M. Graham, S.B. Lee, Experimental considerations on the cytotoxicity of nanoparticles, Nanomedicine (London) 6 (2011) 929–941.
[8] A.A. Selim, A. Al-Sunaidi, N. Tabet, Effect of the surface texture and crystallinity of ZnO nanoparticles on their toxicity, Mater. Sci. Eng. C 32 (2012) 2356–2360.
[9] A.H. Alshehri, M. Jakubowska, A. Młożniak, M. Horaczek, D. Rudka, C. Free, J.D. Carey, Enhanced electrical conductivity of silver nanoparticles for high frequency electronic applications, ACS Appl. Mater. Interfaces 4 (2012) 7007–7010.
[10] D. Shi, M.E. Sadat, A.W. Dunn, D.B. Mast, Photo-fluorescent and magnetic properties of iron oxide nanoparticles for biomedical applications, Nanoscale 7 (2015) 8209–8232.
[11] G.L. Nealon, B. Donnio, R. Greget, J.-P. Kappler, E. Terazzi, J.-L. Gallani, Magnetism in gold nanoparticles, Nanoscale 4 (2012) 5244–5258.
[12] G. Chen, I. Roy, C. Yang, P.N. Prasad, Nanochemistry and nanomedicine for nanoparticle-based diagnostics and therapy, Chem. Rev. 116 (2016) 2826–2885.
[13] E. Fröhlich, The role of surface charge in cellular uptake and cytotoxicity of medical nanoparticles, Int. J. Nanomedicine 7 (2012) 5577–5591.
[14] S. Bhattacharjee, I.M.C.M. Rietjens, M.P. Singh, T.M. Atkins, T.K. Purkait, Z. Xu, S. Regli, A. Shukaliak, R.J. Clark, B.S. Mitchell, G.M. Alink, A.T.M. Marcelis, M.J. Fink, J.G.C. Veinot, S.M. Kauzlarich, H. Zuilhof, Cytotoxicity of surface-functionalized silicon and germanium nanoparticles: the dominant role of surface charges, Nanoscale 5 (2013) 4870–4883.
[15] J.L. Axson, D.I. Stark, A.L. Bondy, S.S. Capracotta, A.D. Maynard, M.A. Philbert, I.L. Bergin, A.P. Ault, Rapid kinetics of size and pH-dependent dissolution and aggregation of silver nanoparticles in simulated gastric fluid, J. Phys. Chem. C 119 (2015) 20632–20641.
[16] E. Blanco, H. Shen, M. Ferrari, Principles of nanoparticle design for overcoming biological barriers to drug delivery, Nat. Biotechnol. 33 (2015) 941–951.
[17] R. Singh, J.W. Lillard, Nanoparticle-based targeted drug delivery, Exp. Mol. Pathol. 86 (2009) 215–223.
[18] H. Takedatsu, K. Mitsuyama, T. Torimura, Nanomedicine and drug delivery strategies for treatment of inflammatory bowel disease, World J. Gastroenterol. 21 (2015) 11343–11352.
[19] S. Ritz, S. Schöttler, N. Kotman, G. Baier, A. Musyanovych, J. Kuharev, K. Landfester, H. Schild, O. Jahn, S. Tenzer, V. Mailänder, Protein corona of nanoparticles: distinct proteins regulate the cellular uptake, Biomacromolecules 16 (2015) 1311–1321.
[20] M. Lundqvist, Nanoparticles: tracking protein corona over time, Nat. Nanotechnol. 8 (2013) 701–702.
[21] M.A. Digman, E. Gratton, Lessons in fluctuation correlation spectroscopy, Annu. Rev. Phys. Chem. 62 (2011) 645–668.
[22] R. Dzakpasu, D. Axelrod, Dynamic light scattering microscopy. A novel optical technique to image submicroscopic motions. I: theory, Biophys. J. 87 (2004) 1279–1287.
[23] A. Kalaitzaki, N.E. Papanikolaou, F. Karamaouna, V. Dourtoglou, A. Xenakis, V. Papadimitriou, Biocompatible colloidal dispersions as potential formulations of natural pyrethrins: a structural and efficacy study, Langmuir 31 (2015) 5722–5730.
[24] A. Satoh, R.W. Chantrell, G.N. Coverdale, Brownian dynamics simulations of ferromagnetic colloidal dispersions in a simple shear flow, J. Colloid Interface Sci. 209 (1999) 44–59.
[25] L. Dalstein, M. Ben Haddada, G. Barbillon, C. Humbert, A. Tadjeddine, S. Boujday, B. Busson, Revealing the interplay between adsorbed molecular layers and gold nanoparticles by linear and nonlinear optical properties, J. Phys. Chem. C 119 (2015) 17146–17155.
[26] J. Lim, S.P. Yeap, H.X. Che, S.C. Low, Characterization of magnetic nanoparticle by dynamic light scattering, Nanoscale Res. Lett. 8 (2013) 381.
[27] A.V. Delgado, F. González-Caballero, R.J. Hunter, L.K. Koopal, J. Lyklema, Measurement and interpretation of electrokinetic phenomena, J. Colloid Interface Sci. 309 (2007) 194–224.
[28] P. Rademeyer, D. Carugo, J.Y. Lee, E. Stride, Microfluidic system for high throughput characterisation of echogenic particles, Lab Chip 15 (2015) 417–428.
[29] Fan, W. Zheng, D.J. Singh, Light scattering and surface plasmons on small spherical particles, Light Sci. Appl. (Nat.) 3 (2014) e179.
[30] D.J. Ross, R. Sigel, Mie scattering by soft core-shell particles and its applications to ellipsometric light scattering, Phys. Rev. E 85 (2012) 056710.
[31] S.-H. Hong, J. Winter, Size dependence of optical properties and internal structure of plasma grown carbonaceous nanoparticles studied by in situ Rayleigh-Mie scattering ellipsometry, J. Appl. Phys. 100 (2006) 064303.
[32] J. Yguerabide, E.E. Yguerabide, Light-scattering submicroscopic particles as highly fluorescent analogs and their use as tracer labels in clinical and biological applications: I. Theory, Anal. Biochem. 262 (1998) 137–156.
[33] Y. Uemura, M. Fujimura, T. Hashimoto, H. Kawai, Application of light scattering from dielectric cylinder based upon Mie and Rayleigh-Gans-Born theories to polymer systems. I. Scattering from a glass fiber, Polym. J. 10 (1978) 341–351.
[34] A. Meller, R. Bar-Ziv, T. Tlusty, E. Moses, J. Stavans, S.A. Safran, Localized dynamic light scattering: a new approach to dynamic measurements in optical microscopy, Biophys. J. 74 (1998) 1541–1548.
[35] B. Lorber, F. Fischer, M. Bailly, H. Roy, D. Kern, Protein analysis by dynamic light scattering: methods and techniques for students, Biochem. Mol. Biol. Educ. 40 (2012) 372–382.
[36] E.L. Gilroy, M.R. Hicks, D.J. Smith, A. Rodger, Viscosity of aqueous DNA solutions determined using dynamic light scattering, Analyst 136 (2011) 4159–4163.
[37] M. Naiim, A. Boualem, C. Ferre, M. Jabloun, A. Jalocha, P. Ravier, Multiangle dynamic light scattering for the improvement of multimodal particle size distribution measurements, Soft Matter 11 (2015) 28–32.
[38] P.S. Santiago, F. Moura, L.M. Moreira, M.M. Domingues, N.C. Santos, M. Tabak, Dynamic light scattering and optical absorption spectroscopy study of pH and temperature stabilities of the extracellular hemoglobin of *Glossoscolex paulistus*, Biophys. J. 94 (2008) 2228–2240.
[39] V. Filipe, A. Hawe, W. Jiskoot, Critical evaluation of nanoparticle tracking analysis (NTA) by NanoSight for the measurement of nanoparticles and protein aggregates, Pharm. Res. 27 (2010) 796–810.
[40] D.S. Bolintineanu, G.S. Grest, J.B. Lechman, F. Pierce, S.J. Plimpton, P.R. Schunk, Particle dynamics modeling methods for colloid suspensions, Comput. Part. Mech. 1 (2014) 321–356.
[41] Y. Min, M. Akbulut, K. Kristiansen, Y. Golan, J. Israelachvili, The role of interparticle and external forces in nanoparticle assembly, Nat. Mater. 7 (2008) 527–538.
[42] A. Lesniak, F. Fenaroli, M.P. Monopoli, C. Åberg, K.A. Dawson, A. Salvati, Effects of the presence or absence of a protein corona on silica nanoparticle uptake and impact on cells, ACS Nano 6 (2012) 5845–5857.
[43] S. Wan, P.M. Kelly, E. Mahon, H. Stöckmann, P.M. Rudd, F. Caruso, K.A. Dawson, Y. Yan, M.P. Monopoli, The "sweet" side of the protein corona: effects of glycosylation on nanoparticle–cell interactions, ACS Nano 9 (2015) 2157–2166.
[44] C.C. Fleischer, C.K. Payne, Nanoparticle–cell interactions: molecular structure of the protein corona and cellular outcomes, Acc. Chem. Res. 47 (2014) 2651–2659.
[45] S. Milani, F. Baldelli Bombelli, A.S. Pitek, K.A. Dawson, J. Rädler, Reversible versus irreversible binding of transferrin to polystyrene nanoparticles: soft and hard corona, ACS Nano 6 (2012) 2532–2541.
[46] W. Liu, J. Rose, S. Plantevin, M. Auffan, J.-Y. Bottero, C. Vidaud, Protein corona formation for nanomaterials and proteins of a similar size: hard or soft corona? Nanoscale 5 (2013) 1658–1668.
[47] S. Lazzari, D. Moscatelli, F. Codari, M. Salmona, M. Morbidelli, L. Diomede, Colloidal stability of polymeric nanoparticles in biological fluids, J. Nanopart. Res. 14 (2012) 920.
[48] S. Khan, A. Gupta, N.C. Verma, C.K. Nandi, Kinetics of protein adsorption on gold nanoparticle with variable protein structure and nanoparticle size, J. Chem. Phys. 143 (2015) 164709.
[49] F. Alexis, E. Pridgen, L.K. Molnar, O.C. Farokhzad, Factors affecting the clearance and biodistribution of polymeric nanoparticles, Mol. Pharm. 5 (2008) 505–515.
[50] A. Salvati, A.S. Pitek, M.P. Monopoli, K. Prapainop, F.B. Bombelli, D.R. Hristov, P.M. Kelly, C. Aberg, E. Mahon, K.A. Dawson, Transferrin-functionalized nanoparticles lose their targeting capabilities when a biomolecule corona adsorbs on the surface, Nat. Nanotechnol. 8 (2013) 137–143.
[51] A. Hawe, W.L. Hulse, W. Jiskoot, R.T. Forbes, Taylor dispersion analysis compared to dynamic light scattering for the size analysis of therapeutic peptides and proteins and their aggregates, Pharm. Res. 28 (2011) 2302–2310.
[52] M.A. Dobrovolskaia, B.W. Neun, S. Man, X. Ye, M. Hansen, A.K. Patri, R.M. Crist, S.E. McNeil, Protein corona composition does not accurately predict hematocompatibility of colloidal gold nanoparticles, Nanomedicine: NBM 10 (2014) 1453–1463.
[53] M. Hadjidemetriou, Z. Al-Ahmady, K. Kostarelos, Time-evolution of *in vivo* protein corona onto blood-circulating PEGylated liposomal doxorubicin (DOXIL) nanoparticles, Nanoscale 8 (2016) 6948–6957.

[54] A.K. Boal, F. Ilhan, J.E. DeRouchey, T. Thurn-Albrecht, T.P. Russell, V.M. Rotello, Self-assembly of nanoparticles into structured spherical and network aggregates, Nature 404 (2000) 746–748.
[55] E.E. Urena-Benavides, C.L. Kitchens, Static light scattering of triaxial nanoparticle suspensions in the Rayleigh-Gans-Debye regime: application to cellulose nanocrystals, RSC Adv. 2 (2012) 1096–1105.
[56] D.W. de Kort, J.P.M. van Duynhoven, H. Van As, F. Mariette, Nanoparticle diffusometry for quantitative assessment of submicron structure in food biopolymer networks, Trends Food Sci. Technol. 42 (2015) 13–26.
[57] K. Ling, H. Jiang, Q. Zhang, A colorimetric method for the molecular weight determination of polyethylene glycol using gold nanoparticles, Nanoscale Res. Lett. 8 (2013) 538.
[58] Online resource from Malvern instruments, http://www.malvern.com/en/products/product-range/zetasizer-range/zetasizer-nano-range/zetasizer-nano-zs/.
[59] Online resource from Brookhaven instruments, http://www.brookhaveninstruments.com/nanodls-laser-light-scattering-instruments.
[60] S. Amin, G.V. Barnett, J.A. Pathak, C.J. Roberts, P.S. Sarangapani, Protein aggregation, particle formation, characterization & rheology, Curr. Opin. Colloid Interface Sci. 19 (2014) 438–449.
[61] Refractive index database, http://refractiveindex.info.
[62] G. Maulucci, M. De Spirito, G. Arcovito, F. Boffi, A.C. Castellano, G. Briganti, Particle size distribution in DMPC vesicles solutions undergoing different sonication times, Biophys. J. 88 (2005) 3545–3550.
[63] Z. Varga, Y. Yuana, A.E. Grootemaat, E. van der Pol, C. Gollwitzer, M. Krumrey, R. Nieuwland, Towards traceable size determination of extracellular vesicles, J. Extracell. Vesicles 3 (2014).
[64] E. Mastan, S. Zhu, A molecular weight distribution polydispersity equation for the ATRP system: quantifying the effect of radical termination, Macromolecules 48 (2015) 6440–6449.
[65] R. Pohl, R. Hauser, M. Li, E. De Souza, R. Feldstein, R. Seibert, K. Ozhan, N. Kashyap, S. Steiner, Ultra-rapid absorption of recombinant human insulin induced by zinc chelation and surface charge masking, J. Diabetes Sci. Technol. 6 (2012) 755–763.
[66] J.A. Finnigan, D.J. Jacobs, Light scattering from benzene, toluene, carbon disulphide and carbon tetrachloride, Chem. Phys. Lett. 6 (1970) 141–143.
[67] D.A. Noday, P.S. Steif, Y. Rabin, Viscosity of cryoprotective agents near glass transition: a new device, technique, and data on DMSO, DP6, and VS55, Exp. Mech. 49 (2009) 663–672.
[68] Guide for DLS sample preparation from Brookhaven instruments, http://www.brookhaveninstruments.com/pdf/theory/Guide_for_DLS_sample_preparation.pdf.
[69] R. Chanamai, D.J. McClements, Creaming stability of flocculated monodisperse oil-in-water emulsions, J. Colloid Interface Sci. 225 (2000) 214–218.
[70] J. Panchal, J. Kotarek, E. Marszal, E.M. Topp, Analyzing subvisible particles in protein drug products: a comparison of dynamic light scattering (DLS) and resonant mass measurement (RMM), AAPS J. 16 (2014) 440–451.
[71] K.H. Müller, M. Motskin, A.J. Philpott, A.F. Routh, C.M. Shanahan, M.J. Duer, J.N. Skepper, The effect of particle agglomeration on the formation of a surface-connected compartment induced by hydroxyapatite nanoparticles in human monocyte-derived macrophages, Biomaterials 35 (2014) 1074–1088.
[72] T. Zheng, P. Cherubin, L. Cilenti, K. Teter, Q. Huo, A simple and fast method to study the hydrodynamic size difference of protein disulfide isomerase in oxidized and reduced form using gold nanoparticles and dynamic light scattering, Analyst 141 (2016) 934–938.
[73] A.R. Karow, J. Götzl, P. Garidel, Resolving power of dynamic light scattering for protein and polystyrene nanoparticles, Pharm. Dev. Technol. 20 (2015) 84–89.
[74] Z. Meng, S.M. Hashmi, M. Elimelech, Aggregation rate and fractal dimension of fullerene nanoparticles via simultaneous multiangle static and dynamic light scattering measurement, J. Colloid Interface Sci. 392 (2013) 27–33.
[75] C. Gei, A. Gollwitzer, C. Sikora, M. Minelli, U. Krumrey, Resch-Genger, effect of fluorescent staining on size measurements of polymeric nanoparticles using DLS and SAXS, Anal. Methods 7 (2015) 9785–9790.
[76] R.C. Murdock, L. Braydich-Stolle, A.M. Schrand, J.J. Schlager, S.M. Hussain, Characterization of nanomaterial dispersion in solution prior to *in vitro* exposure using dynamic light scattering technique, Toxicol. Sci. 101 (2008) 239–253.
[77] H.H. Liu, S. Surawanvijit, R. Rallo, G. Orkoulas, Y. Cohen, Analysis of nanoparticle agglomeration in aqueous suspensions via constant-number Monte Carlo simulation, Environ. Sci. Technol. 45 (2011) 9284–9292.
[78] W.H. De Jong, P.J.A. Borm, Drug delivery and nanoparticles: applications and hazards, Int. J. Nanomedicine 3 (2008) 133–149.
[79] C. Zhou, W. Qi, E. Neil Lewis, J.F. Carpenter, Concomitant Raman spectroscopy and dynamic light scattering for characterization of therapeutic proteins at high concentrations, Anal. Biochem. 472 (2015) 7–20.
[80] W. Niu, Y.A.A. Chua, W. Zhang, H. Huang, X. Lu, Highly symmetric gold nanostars: crystallographic control and surface-enhanced Raman scattering property, J. Am. Chem. Soc. 137 (2015) 10460–10463.
[81] Q. Zhang, J.-Q. Huang, W.-Z. Qian, Y.-Y. Zhang, F. Wei, The road for nanomaterials industry: a review of carbon nanotube production, post-treatment, and bulk applications for composites and energy storage, Small 9 (2013) 1237–1265.
[82] N. Nair, W.-J. Kim, R.D. Braatz, M.S. Strano, Dynamics of surfactant-suspended single-walled carbon nanotubes in a centrifugal field, Langmuir 24 (2008) 1790–1795.
[83] T.-C. Lee, M. Alarcón-Correa, C. Miksch, K. Hahn, J.G. Gibbs, P. Fischer, Self-propelling nanomotors in the presence of strong Brownian forces, Nano Lett. 14 (2014) 2407–2412.
[84] NIST guidelines on sample preparation, http://ncl.cancer.gov/NCL_Method_NIST-NCL_PCC-1.pdf.
[85] M. Kaszuba, M.T. Connah, F.K. McNeil-Watson, U. Nobbmann, Resolving concentrated particle size mixtures using dynamic light scattering, Part. Part. Syst. Charact. 24 (2007) 159–162.
[86] M. de Kanter, J. Meyer-Kirschner, J. Viell, A. Mitsos, M. Kather, A. Pich, C. Janzen, Enabling the measurement of particle sizes in stirred colloidal suspensions by embedding dynamic light scattering into an automated probe head, Measurement 80 (2016) 92–98.
[87] M. Bouri, R. Salghi, M. Algarra, M. Zougagh, A. Rios, A novel approach to size separation of gold nanoparticles by capillary electrophoresis-evaporative light scattering detection, RSC Adv. 5 (2015) 16672–16677.
[88] F. Duan, D. Kwek, A. Crivoi, Viscosity affected by nanoparticle aggregation in Al_2O_3-water nanofluids, Nanoscale Res. Lett. 6 (2011) 1–5.
[89] M. Grouchko, P. Roitman, X. Zhu, I. Popov, A. Kamyshny, H. Su, S. Magdassi, Merging of metal nanoparticles driven by selective wettability of silver nanostructures, Nat. Commun. 5 (2014).
[90] H. Hagendorfer, R. Kaegi, M. Parlinska, B. Sinnet, C. Ludwig, A. Ulrich, Characterization of silver nanoparticle products using asymmetric flow field flow fractionation with a multidetector approach – a comparison to transmission electron microscopy and batch dynamic light scattering, Anal. Chem. 84 (2012) 2678–2685.
[91] X. Zhao, S. Zhu, Y. Song, J. Zhang, B. Yang, Thermal responsive fluorescent nanocomposites based on carbon dots, RSC Adv. 5 (2015) 15187–15193.
[92] K.-H. Kim, H. Xing, J.-M. Zuo, P. Zhang, H. Wang, TEM based high resolution and low-dose scanning electron nanodiffraction technique for nanostructure imaging and analysis, Micron 71 (2015) 39–45.
[93] G. Zhou, J.C. Yang, In situ UHV-TEM investigation of the kinetics of initial stages of oxidation on the roughened Cu(110) surface, Surf. Sci. 559 (2004) 100–110.
[94] E.D.H. Mansfield, K. Sillence, P. Hole, A.C. Williams, V.V. Khutoryanskiy, POZylation: a new approach to enhance nanoparticle diffusion through mucosal barriers, Nanoscale 7 (2015) 13671–13679.
[95] P. Klapetek, M. Valtr, D. Nečas, O. Salyk, P. Dzik, Atomic force microscopy analysis of nanoparticles in non-ideal conditions, Nanoscale Res. Lett. 6 (2011) 1–9.
[96] C. Lamprecht, P. Hinterdorfer, A. Ebner, Applications of biosensing atomic force microscopy in monitoring drug and nanoparticle delivery, Expert Opin. Drug Deliv. 11 (2014) 1237–1253.
[97] L.A. Fielding, O.O. Mykhaylyk, S.P. Armes, P.W. Fowler, V. Mittal, S. Fitzpatrick, Correcting for a density distribution: particle size analysis of core–shell nanocomposite particles using disk centrifuge photosedimentometry, Langmuir 28 (2012) 2536–2544.
[98] Guideline on DCS from CPS instruments, http://www.cpsinstruments.eu/pdf/Introduction%20Differential%20Sedimentation.pdf.
[99] Ž. Krpetić, A.M. Davidson, M. Volk, R. Lévy, M. Brust, D.L. Cooper, High-resolution sizing of monolayer-protected gold clusters by differential centrifugal sedimentation, ACS Nano 7 (2013) 8881–8890.
[100] J. Ziegler, H. Wachtel, Comparison of cascade impaction and laser diffraction for particle size distribution measurements, J. Aerosol Med. 18 (2005) 311–324.
[101] A.C. Sabuncu, J. Grubbs, S. Qian, T.M. Abdel-Fattah, M.W. Stacey, A. Beskok, Probing nanoparticle interactions in cell culture media, Colloids Surf. B: Biointerfaces 95 (2012) 96–102.
[102] G. Maiorano, S. Sabella, B. Sorce, V. Brunetti, M.A. Malvindi, R. Cingolani, P.P. Pompa, Effects of cell culture media on the dynamic formation of protein–nanoparticle complexes and influence on the cellular response, ACS Nano 4 (2010) 7481–7491.
[103] R.P. Singh, V.K. Jaiswal, V.K. Jain, Study of smoke aerosols under a controlled environment by using dynamic light scattering, Appl. Opt. 45 (2006) 2217–2221.
[104] D.J. Durian, D.A. Weitz, D.J. Pine, Multiple light-scattering probes of foam structure and dynamics, Science 252 (1991) 686–688.
[105] M. Kaszuba, J. Corbett, F.M. Watson, A. Jones, High-concentration zeta potential measurements using light-scattering techniques, Philos. Transact. A Math. Phys. Eng. Sci. 368 (2010) 4439–4451.
[106] F.J. Montes Ruiz-Cabello, G. Trefalt, P. Maroni, M. Borkovec, Electric double-layer potentials and surface regulation properties measured by colloidal-probe atomic force microscopy, Phys. Rev. E 90 (2014) 012301.
[107] Z. Chen, Z. Wei, Y. Chen, C. Dames, Anisotropic Debye model for the thermal boundary conductance, Phys. Rev. B 87 (2013) 125426.
[108] F.J. Vidal-Iglesias, J. Solla-Gullón, A. Rodes, E. Herrero, A. Aldaz, Understanding the Nernst equation and other electrochemical concepts: an easy experimental approach for students, J. Chem. Educ. 89 (2012) 936–939.
[109] H. Thakkar, J. Nangesh, M. Parmar, D. Patel, Formulation and characterization of lipid-based drug delivery system of raloxifene-microemulsion and self-microemulsifying drug delivery system, J. Pharm. Bioallied Sci. 3 (2011) 442–448.
[110] T. Ito, L. Sun, M.A. Bevan, R.M. Crooks, Comparison of nanoparticle size and electrophoretic mobility measurements using a carbon-nanotube-based coulter counter, dynamic light scattering, transmission electron microscopy, and phase analysis light scattering, Langmuir 20 (2004) 6940–6945.
[111] V.N. Shilov, Y.B. Borkovskaja, A.S. Dukhin, Electroacoustic theory for concentrated colloids with overlapped DLs at arbitrary κa: I. Application to nanocolloids and nonaqueous colloids, J. Colloid Interface Sci. 277 (2004) 347–358.
[112] V. Uskoković, Z. Castiglione, P. Cubas, L. Zhu, W. Li, S. Habelitz, Zeta-potential and particle size analysis of human amelogenins, J. Dent. Res. 89 (2010) 149–153.
[113] J. Kirkwood, D. Hargreaves, S. O'Keefe, J. Wilson, Using isoelectric point to determine the pH for initial protein crystallization trials, Bioinformatics 31 (2015) 1444–1451.
[114] A. Salis, M. Boström, L. Medda, F. Cugia, B. Barse, D.F. Parsons, B.W. Ninham, M. Monduzzi, Measurements and theoretical interpretation of points of zero charge/potential of BSA protein, Langmuir 27 (2011) 11597–11604.
[115] E.W. Nägele, The transient zeta potential of hydrating cement, Chem. Eng. Sci. 44 (1989) 1637–1645.
[116] V.R. Patel, Y.K. Agrawal, Nanosuspension: an approach to enhance solubility of drugs, J. Adv. Pharm. Technol. Res. 2 (2011) 81–87.

[117] T. Missana, A. Adell, On the applicability of DLVO theory to the prediction of clay colloids stability, J. Colloid Interface Sci. 230 (2000) 150–156.
[118] F.L. Leite, C.C. Bueno, A.L. Da Róz, E.C. Ziemath, O.N. Oliveira, Theoretical models for surface forces and adhesion and their measurement ssing atomic force microscopy, Int. J. Mol. Sci. 13 (2012) 12773–12856.
[119] K.-M. Kim, H.M. Kim, W.-J. Lee, C.-W. Lee, T.-i. Kim, J.-K. Lee, J. Jeong, S.-M. Paek, J.-M. Oh, Surface treatment of silica nanoparticles for stable and charge-controlled colloidal silica, Int. J. Nanomedicine 9 (2014) 29–40.
[120] T.C.A. Almeida, A.L. Larentis, H.C. Ferraz, Evaluation of the stability of concentrated emulsions for lemon beverages using sequential experimental designs, PLoS One 10 (2015) e0118690.
[121] H. Kouchakzadeh, S.A. Shojaosadati, A. Maghsoudi, E. Vasheghani Farahani, Optimization of PEGylation conditions for BSA nanoparticles using response surface methodology, AAPS PharmSciTech 11 (2010) 1206–1211.
[122] P.P. Pillai, B. Kowalczyk, W.J. Pudlo, B.A. Grzybowski, Electrostatic titrations reveal surface compositions of mixed, on-nanoparticle monolayers comprising positively and negatively charged ligands, J. Phys. Chem. C 120 (2016) 4139–4144.
[123] A. Clavier, M. Seijo, F. Carnal, S. Stoll, Surface charging behavior of nanoparticles by considering site distribution and density, dielectric constant and pH changes - a Monte Carlo approach, Phys. Chem. Chem. Phys. 17 (2015) 4346–4353.
[124] M. Di Marco, C. Sadun, M. Port, I. Guilbert, P. Couvreur, C. Dubernet, Physicochemical characterization of ultrasmall superparamagnetic iron oxide particles (USPIO) for biomedical application as MRI contrast agents, Int. J. Nanomedicine 2 (2007) 609–622.
[125] Y. Hedberg, X. Wang, J. Hedberg, M. Lundin, E. Blomberg, I. Odnevall Wallinder, Surface-protein interactions on different stainless steel grades: effects of protein adsorption, surface changes and metal release, J. Mater. Sci. Mater. Med. 24 (2013) 1015–1033.
[126] I.M. Tucker, J.C.W. Corbett, J. Fatkin, R.O. Jack, M. Kaszuba, B. MacCreath, F. McNeil-Watson, Laser Doppler electrophoresis applied to colloids and surfaces, Curr. Opin. Colloid Interface Sci. 20 (2015) 215–226.
[127] P. Satzer, F. Svec, G. Sekot, A. Jungbauer, Protein adsorption onto nanoparticles induces conformational changes: particle size dependency, kinetics, and mechanisms, Eng. Life Sci. 16 (2016) 238–246.
[128] M.A. Dobrovolskaia, S.E. McNeil, Understanding the correlation between *in vitro* and *in vivo* immunotoxicity tests for nanomedicines, J. Control. Release 172 (2013) 456–466.
[129] J.A. Kim, A. Salvati, C. Aberg, K.A. Dawson, Suppression of nanoparticle cytotoxicity approaching *in vivo* serum concentrations: limitations of *in vitro* testing for nanosafety, Nanoscale 6 (2014) 14180–14184.
[130] Y. Lu, S. Kim, K. Park, *In vitro-in vivo* correlation: perspectives on model development, Int. J. Pharm. 418 (2011) 142–148.